Vibration in Gemini and Engineering modifications (interim report).

Contact *steve.blake@stfc.ac.uk*

Stephen Blake
STFC, Central Laser Facility
RAL, OX11 0QX

Houcheng Huang
Diamond
RAL OX11 0QX

Rajeev Pattathil
STFC, Central Laser Facility
RAL, OX11 0QX

Peta Foster
STFC, Central Laser Facility
RAL, OX11 0QX

Introduction

Astra Gemini is a dual beam facility with each beam delivering 0.5PW energy in 30fs every 60 seconds. Gemini is housed in building R7, the seed beam comes from Astra and is split, amplified and compressed above the Target Area then delivered through the bunker roof (300mm thick concrete) into the Target Area. In the Target Area each beam propagates off a number of mirrors to be focused to a 2-20 micron spot at the interaction point where they interact with extremely delicate targets which are vaporised. Experiments can utilise both beams interacting together and this requires a highly stable and synchronised system in both space and time.

Vibration was observed within the target area that affected both the internal and external laser beam pointing stability. The observed motion of the focal spot depended on the nature of the focussing geometry but often created a very stable elliptical or *figure of eight* movement of the spot. This was observed to disappear completely during maintenance periods in ISIS when the main magnet power supply was switched off. The motion produced by the vibration was observed to be about 6-10 spot diameters. This degree of motion is detrimental for most experiments and catastrophic for any dual beam spatially synchronised operation.

ISIS has a number of different systems used to generate the stable 50Hz power required to run. A generator is used predominately with a backup system employing a UPS. To determine the exact source observations were carried out with the generator running and the UPS running. No obvious difference was observed ruling the generator out as the source. Physical inspection of the choke and area round the choke identified a strong vibration which propagated into R6. The choke is one of the main power components for the magnets that form the synchrotron.

Figure 1 shows a simplified site plan identifying the relationship between the Gemini Target Area and the choke. The choke is just outside building R6 and tunnel 7 joins building R6 to building R7. Figure 2 shows a plan view from Google Maps identifying the same buildings and the area of the tunnel. Figure 3 shows the target chamber mounted directly over the trench leading directly to tunnel 7. Both the breadboard support frame and the chamber support frame straddle the trench. The mounting positions directly over the trench are unused and are clear of the trench covers. Tunnel 7 is a concrete structure approx 2.5m high and 2m wide inside and is used for services infrastructure. The whole of the site is built on a chalk bed and recent tests on the chalk 100m away from building R7 suggest the chalk is nearly as dense as structural concrete.

The vibration was observed on the monitors connected to the alignment microscopes which are used to align the beam to the target.

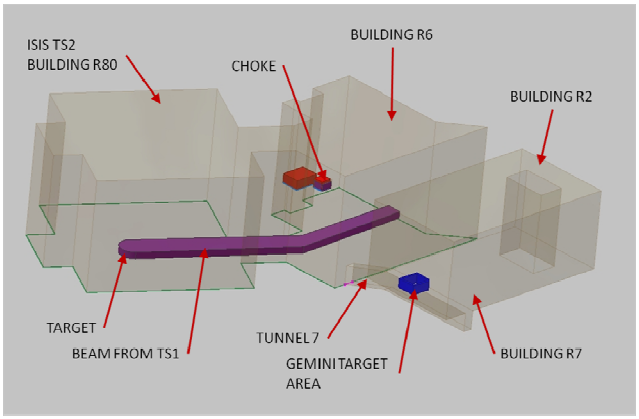

Figure 1-Relationship between the choke and target area

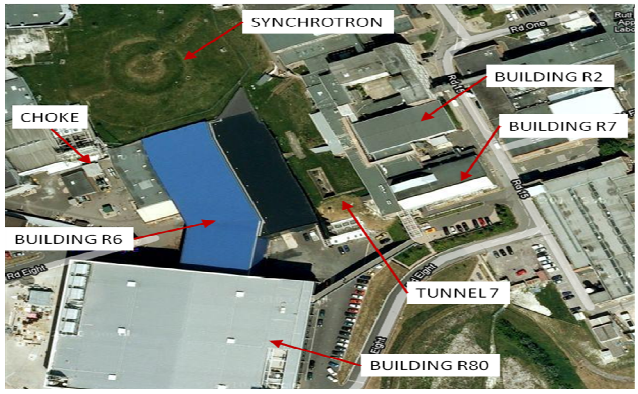

Figure 2-Plan view from Google Maps of the area.

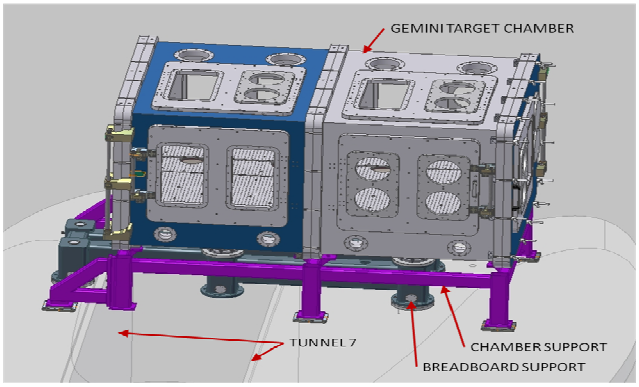

Figure 3-Relationship between the target chamber and tunnel 7

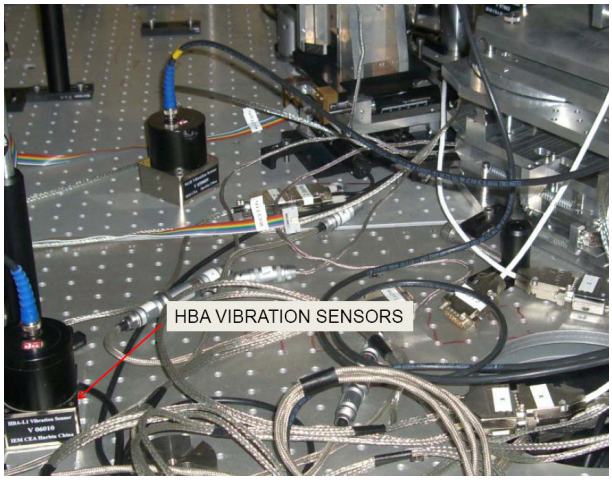

Figure 4-Vibration measurement being carried out inside the Gemini Interaction Chamber

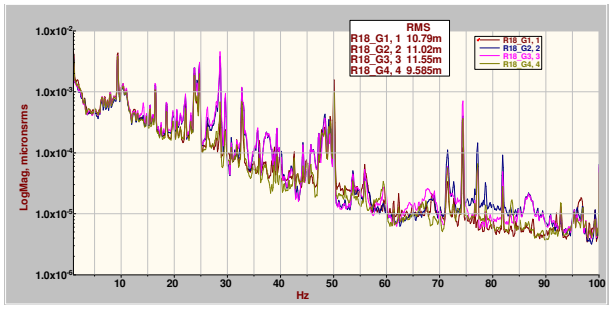

Figure 5-Frequency spectrum measured in the Target Area with ISIS off.

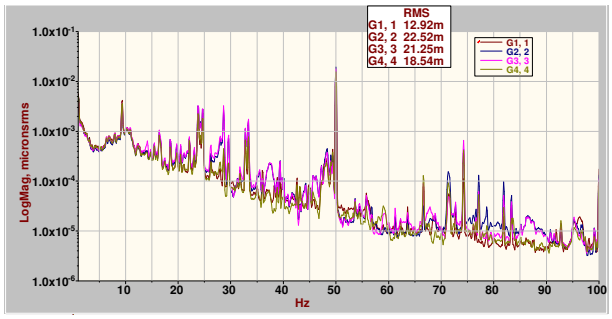

Figure 6-Frequency Spectrum measured in the Target Area with ISIS on.

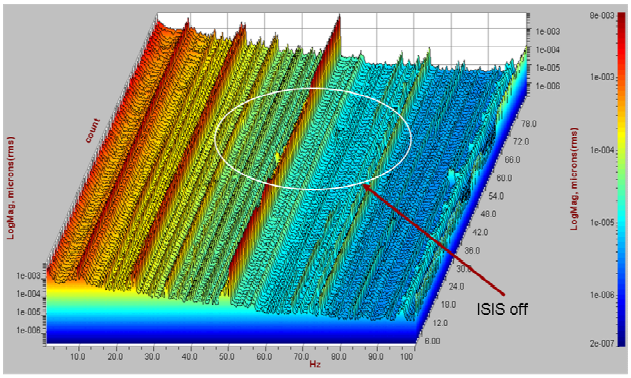

Figure 7-Spectrum plot of one sensor showing ISIS switch off and the corresponding change.

Vibration Survey

A vibration survey was carried out in collaboration with Houch-Eng Huang in Diamond. Figure 4 shows the HBA sensors measuring positions on the breadboard. These sensors are used routinely in Diamond around the ring and the sensor design is optimised for sensitivity to ground borne vibration down to 0.5Hz.

Figures 5 & 6 show plots of the spectrum with ISIS on and ISIS off. There is a clear increase in the spike at 50Hz and a number of other spikes that appear around 30Hz and 70Hz. Figure 7 shows a direct comparison of displacement against time for one sensor with and without ISIS. The signal propagated is only visible in the vertical plane.

Figure 8 shows the spot movement of a He Ne laser propagated off a number of mirrors both in the target area and in the interaction chamber itself. The spot position was recorded over several milliseconds with a lateral effect position sensitive detector. A Fourier analysis reveals a strong 50Hz component as identified in the other vibration measurements. It should be noted that the movement is much more pronounced in the horizontal direction but could still be caused by vertical ground borne vibration due to the complicated beam path involving periscopes. Further investigation is underway.

Considered methods to overcome the problem.

1. The laser could be synchronised with the ISIS 50Hz power supply making the laser fire at the same exact time in the cycle allowing alignment. The CW beam would additionally be pulsed with the 50Hz so that it also appeared to be stationary.

2. Investigate the TA hardware to identify items with a natural frequency at 50Hz.

3. Isolate the chamber from the source with Sorbothane, a material known for its damping characteristics.

4. Isolate the source of the ground borne vibration.

5. Break the main path to the chamber with a trench.

6. Stiffen all the structure so that it performs as a single entity.

(1) The effort and cost required to synchronise with ISIS was small and this was the first step.

(2) Initial tests on the chamber components were carried out using a SKF RT440 looking for a significant increase in 50Hz amplitude throughout the structures. Initial testing suggested the signal was amplified through the breadboard structure and further amplified through the parabola mounts.

(3) Isolating the breadboard in the chamber was ruled out. The ground borne vibration was measured throughout the bunker. With the whole bunker being used to support hardware in the laser chain it is expected that isolating one item would only move the problem to manifest itself somewhere else. Additionally major work on the breadboard would require a complete strip of the area which would see a shutdown of >6 months. This would have a serious impact on operations and was deemed unfeasible.

(4) The source is significant hardware at the heart of ISIS. Isolating this is not feasible. It is currently identified as an area of single point failure as is no longer commercially available. A replacement unit is in construction in building R6 forming 8-10 smaller units. Commissioning is planned later this year but the impact is difficult to determine.

(5) Breaking the path with a trench is not feasible due to there being no practical location for the break. The cost and impact to operations caused by the work would be significant.

(6) Stiffening the structure is possible and feasible.

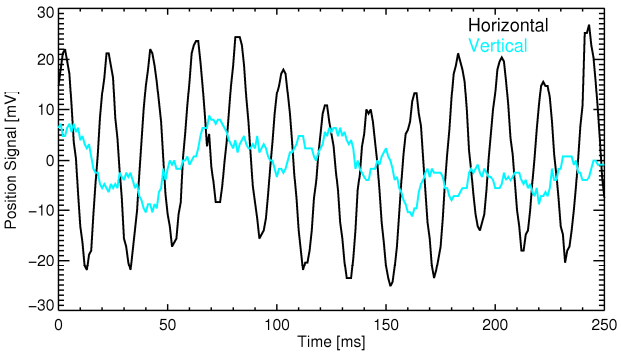

Figure 8-Spot movement of a He Ne laser propagated in the Target Area.

Components with a natural frequency of 50Hz

The Parabola mounts were both found to amplify the 50Hz signal and were dispatched to TUV for full spectrum testing. Figure 9 shows the mount on test on a shaker table. The mount is designed to align the parabola and is a high accuracy five stage translation and rotation stage utilising high precision commercially available motor micrometers with zero backlash.

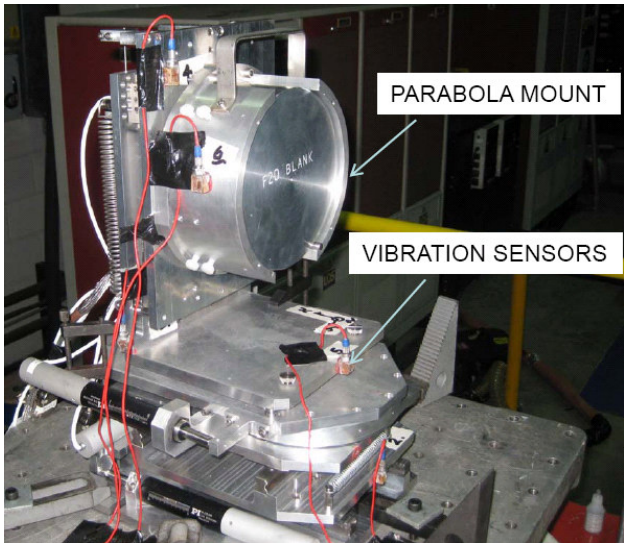

Figure 9-Parabola mount under test at TUV.

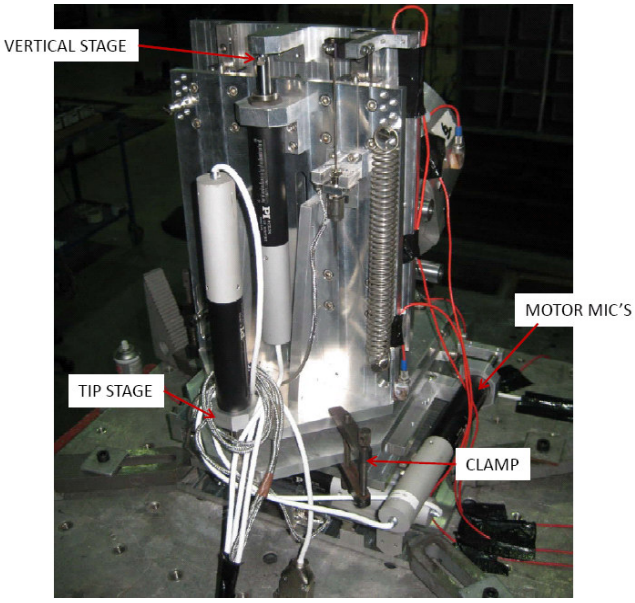

Figure 10-Tip and Vertical stages shown to be sensitive.

Figure 10 shows the back of the mount where the vertical and tip stages are located. The clamp shown was used to methodically stiffen the mount allowing re-runs to identify the sensitivity to vertical vibration in each stage. The mount has two different configurations depending on its location within the Interaction Chamber. Both were tested with sweeps up to 105Hz using the lowest input "g" level the machine could to register a signal. Figure 11 shows the control channel at 0.03g.

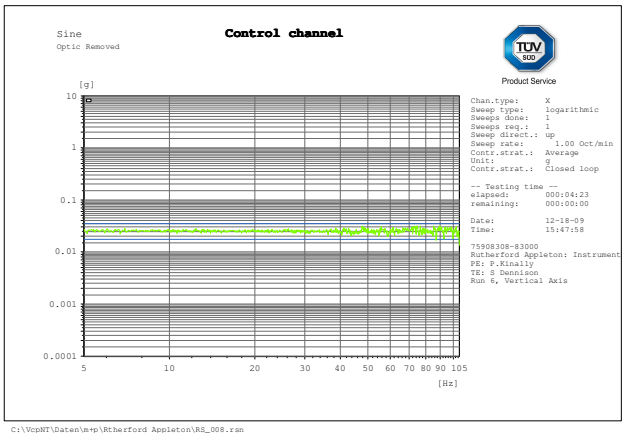

Figure 11-Shaker rig control channel at 0.03g

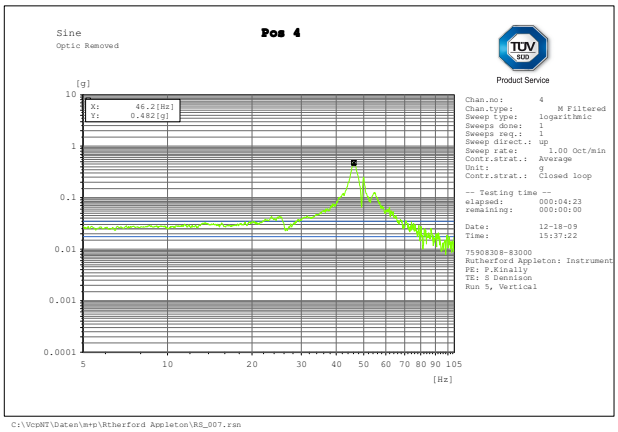

Figure 12-Shaker rig scan identifying problems in Tip Stage.

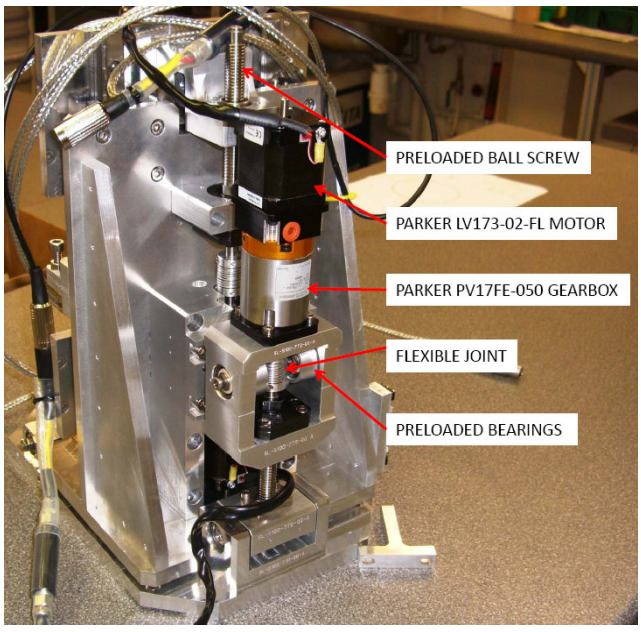

Figure 13-New parabola mount tip and vertical stages.

Figure 12 shows the tip stage having a natural frequency at around 46Hz and 50Hz. The vertical stage had a similar graph at 50Hz.

The original design intent was to manufacture an extremely compact mount capable of being positioned side by side to allow both 0.5PW beams to be focussed on target using commercially available hardware with zero backlash. To overcome the 50Hz natural frequency it was obvious a re-design stiffening the tip and vertical stages was necessary. Figure 13 shows the new design implemented. The two Pi motor micrometers have been replaced by high precision preloaded ball screws from THK. The Parker motor and gearbox are similar to that used in other areas across the facility without problem. The preloaded bearings were purchased from Carter bearings. With preloaded bearings and preloaded ball screws it is expected that the stiffness in the vertical direction will be significantly increased.

Stiffen all the breadboard structures

The design intent for the breadboard in the Interaction Chamber was for it to be populated and aligned with optics offline allowing a faster turnaround of experiments and more experimental output. The breadboards were split up into four separate pieces. This is shown in figure 14. The four separate breadboards were bolted to two separate intermediate frames then to the main sub-frame. Initial analysis suggested that this structure amplified the 50Hz signal and therefore had a corresponding natural frequency.

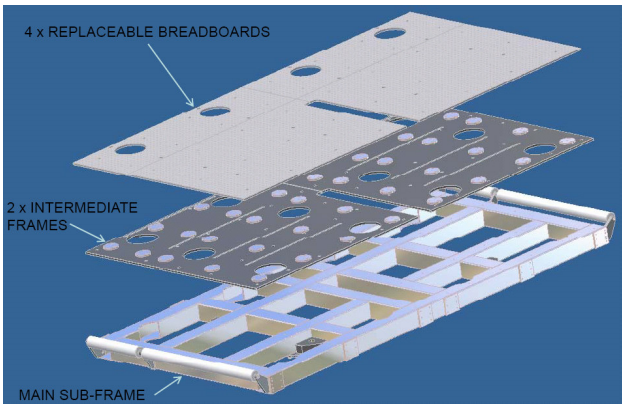

Figure 14-Initial breadboard construction

Time was short for a detailed investigation and the decision was made to consolidate all the components into one single structure shown in figure 15. The support legs were also revised to improve the installation procedure. The 7075 aluminium had a longer lead time over cast tooling plate but 7075 offers better scratch resistance over cast tooling plate and offers longer wear for the threads. 7075 aluminium suffers from its notch sensitivity leading to crack propagation however its notch sensitivity would not be a weakness in this design.

Figure 16 shows the long focal length parabola chamber which houses a parabola mount and the F20 optic. This assembly was stiffened by increasing the thickness of the floor plate, stiffening the support frame and introducing bellows to reduce the bending caused by the deflection in the main chamber during pump down.

Further stiffening was carried out by casting the support structures to the floor using Fosroc Conbextra EPR for the larger structure and Fosroc Conbextra EPLV for the feet.

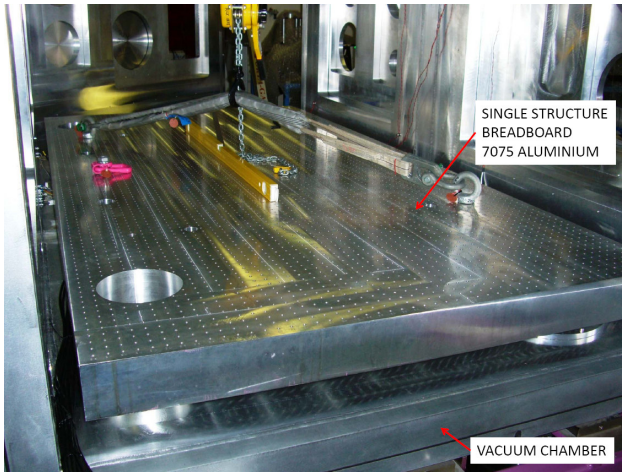

Figure 15-Revised single structure breadboard

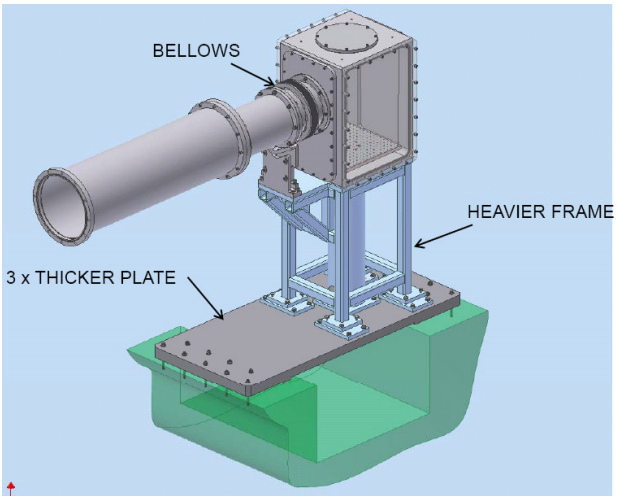

Figure 16-revised structure for the long focal length parabola

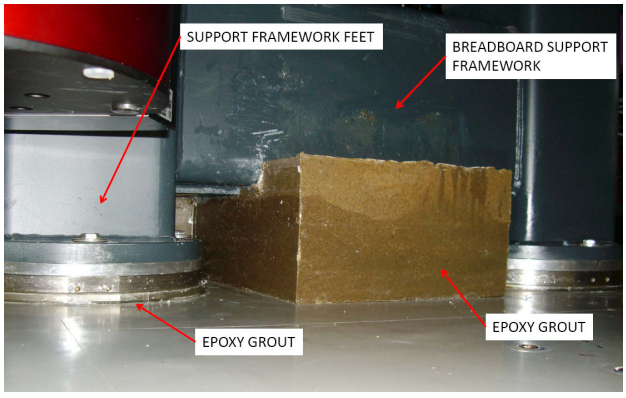

Figure 17-The breadboard support structure is cast to the floor

The EBR variant is a loaded two part epoxy compound and McNaughton Bailey Ltd were employed to weir up the structure and pour the material over a weekend. The trench limited the length of the pour which extends from the east side shown in figure 17 to the edge of the trench. Stopping at the trench ensures continued access for services. The EPLV material is a very low viscosity two part epoxy which was flooded in around the feet ensuring a good connection to the concrete substrate below.

Analysis of the revised structure

Figure 18 shows the location of the vibration sensors for the plot on figure 19. Sensor 4 is assumed to be the reference as the structure is now bonded to the floor. Sensors 1-3 are therefore measuring any amplification of the signal through the structure. Although the breadboard structure was replaced it was not possible to make any structural changes to the four support legs without dismantling the chamber. Figure 19 shows the spectrum with ISIS switched on. There is a marked reduction in the background over the initial scans. Sensors 1 & 3 produce an identical trace and show only a slight increase over the reference. Sensor 2 shows a further increase that could suggest that the trench is the main conduit for the vibration or that further stiffening of the structure above the trench could provide further gains.

Conclusions

Replacing the breadboard with a single structure, grouting the breadboard support to the ground and reinforcing the long focal length parabola have all significantly reduced the background noise, but as expected the main peaks from ISIS are unaffected.

The single breadboard eliminates the previous local problems where components spanned two sections of the breadboard. Initial experimental operations on the new structure suggest the structural changes are positive. The changes to the parabola mounts are expected to have a significant improvement again. The area is operational preventing the new parabola mounts being installed and they are on standby should there be problems with the current mounts prevent them from being tested on the shaker table.

All areas on site see ground borne vibration from ISIS, Diamond and traffic on the A34. In this particular area we had structure that was sensitive to 50Hz. Following the design philosophy included herein should prevent the need for expensive computer analysis on all future designs.

This is an interim report pending the results of the vibration sweep of the new parabola mount design and final testing in the vacuum chamber. Final conclusions will be in next year's report.

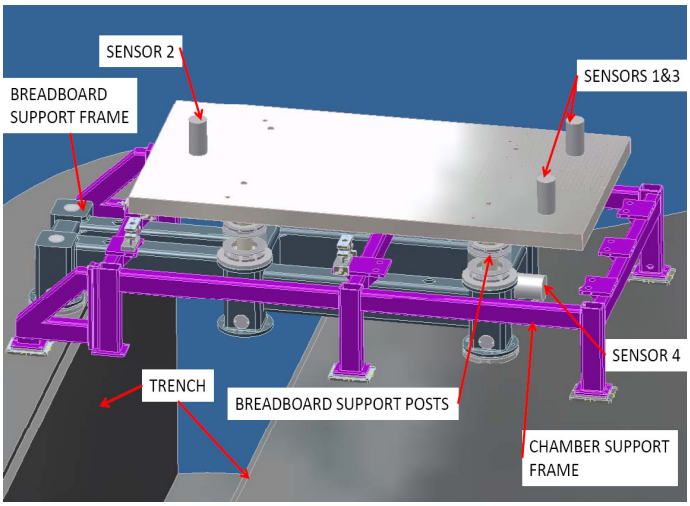

Figure 18-Showing the new structure and the location of the four sensors

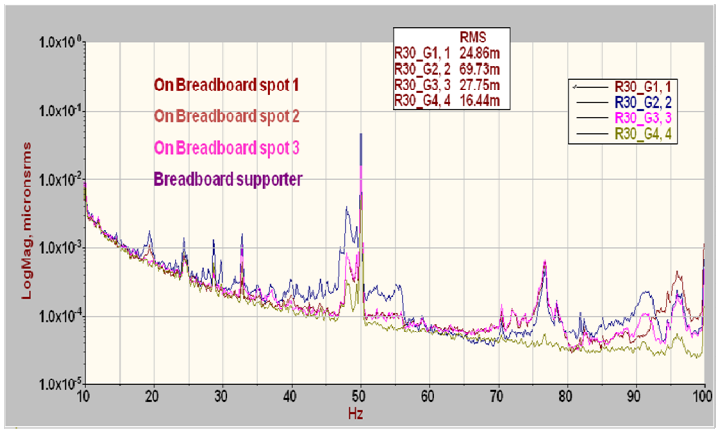

Figure 19-Measurements taken of new breadboard structure

Temporal and Spatial Overlap Monitoring of the Dual-Beam Layout in Astra-Gemini TA3

Contact *nicola.booth@stfc.ac.uk*

N. Booth, D. R. Symes, P. S. Foster, J. Martin, P. P. Rajeev, D. Neely

Central Laser Facility, STFC, Rutherford Appleton Laboratory, HSIC, Didcot, Oxon, OX11 0QX

Introduction

The Astra-Gemini target area has been operational for user experiments since 2008 in a single beam configuration. The laser system is now up and running for dual beam experiments. In order to meet the requirements for users with small focal spot sizes (~ few microns) and femtosecond pulse durations it is now critical for the outcome of experiments that the spatial and temporal overlap of the two beams at the target position. Here we report on two newly implemented diagnostics in the target area to monitor the overlap (both spatially and temporally) of the two beams.

Astra-Gemini TA3

The current experimental set-up is to have the two beams of the Gemini system focused onto target with the *f*/20 parabola on the south beam, focusing to a spot of ~ 30 µm and the north beam focused with an *f*/2 parabola, giving a spot of ~2 µm. The pulses are compressed to pulse durations of ~ 40 fs. With the implementation of the first dual beam experiment using Astra-Gemini, the size of the focal spots and the ultra-short pulse duration of the system means that the need to have shot-to-shot measurements of the spatial and temporal overlap of the two beams is of extreme importance. These extra diagnostics are added into the existing TA3 beam diagnostics which use the leakage through the rear of one dielectric mirror in each of the beam lines. A schematic diagram of existing and planned beam diagnostics is shown in Fig. 1. For each experimental arrangement, once zero delay between the main beams has been set up, the delay in the south diagnostic line can be adjusted to reset the temporal overlap monitor.

Beam Overlap Diagnostic

For the first overlap diagnostic, two leakage beams are combined using a dielectric beamsplitter inside the target chamber after the minimum possible number of optics. Because very little energy is needed we pick off a ~1cm beam from the unfocussed mirror leakage. The combined beam is directed to a system above the target chamber built with caged opto-mechanics to increase stability, shown in Fig. 2(a). The beam is focused using an *f*/20 lens and split onto a pre-focus near-field camera and a far-field camera with a microscope objective. A slight adjustment on one of the diagnostic beams then produces two closely spaced but distinct focal spots and interference fringes in the near field.

Once the beams are combined, vibrations in the common optics are not important since we need to monitor only the relative positions of the two focal spots. It will be necessary to check whether instabilities in the leakage beam focal positions correspond exactly to those in the main beam focal spots.

The far-field camera will measure the shot-to-shot spatial stability of the two beams. Software will be developed to monitor the positions of the spots and later to provide feedback to a pointing mirror to allow for automatic correction of beam drift.

The visibility of a near-field interference pattern will be an accurate indicator of a temporal overlap between the two beams of less than the pulse envelope duration. It will also be sensitive to jitter in the spatial alignment since this will alter the fringe pattern.

Cross-correlator diagnostic

The second method to monitor the temporal overlap is to measure a cross-correlation signal between the two leakage beams (Fig 2(b)). This requires an energy ~1mJ so we down-collimate the leakage beams using a telescope with magnification -15 (the same focusing lens as used for the main beam equivalent plane monitor). The beams are then split and overlapped in two separate BBO crystals to generate two cross-correlation traces, imaged without magnification to CCD cameras. At the zero-delay position this gives a centred vertical stripe. Any change in delay between the beams moves this stripe, the direction depending on which beam comes earlier.

One of the correlators has a 'tight' crossing angle which provides a time-window of ~6ps. A shift in the delay stage of 10µm, corresponding to a delay <100fs, is clearly detectable on this camera. The second arrangement has a wider time window to measure delays of >6ps, lying outside the window of the 'accurate' timing correlator. Delays >50ps can be measured using a fast photodiode (35ps rise time).

We intend to write software to capture the central position of the correlation trace on each shot providing a shot-to-shot measurement of temporal stability. This could also be incorporated into a feedback system to the delay stage in LA3 to correct for timing drift during the day.

Conclusions

The beginning of dual beam operations on Astra-Gemini required additional beam diagnostic to monitor beam overlap. We have started to implement such systems and will start to operate them on full power shots in the next few months. It should be possible to use these diagnostics to implement a feedback system to correct for beam drifts.

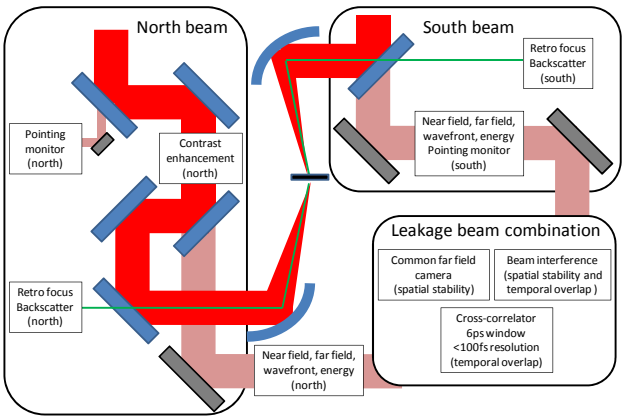

Figure 1: Schematic diagram of the beam arrangements in Astra-Gemini TA3. Red indicates the main beamlines and pink indicates leakage beams.

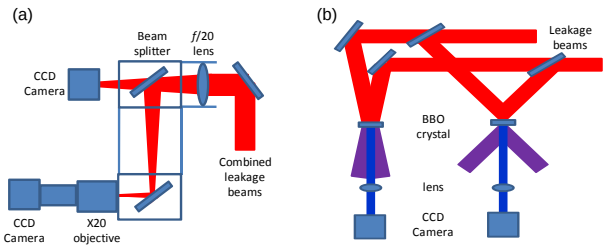

Figure 2: Schematic diagram of (a) the combined beam near and far-field diagnostic and (b) the double cross-correlator arrangement.

Upgrade of Astra Amplifier 3 and the Astra interlock system

Contact *chris.hooker@stfc.ac.uk*

Chris Hooker, Billy Costello, Steve Hawkes, Chris John, Brian Landowski, Andy Tylee

Central Laser Facility, Rutherford Appleton Laboratory
Chilton, Oxfordshire OX11 0QX

Introduction

The multi-terawatt Amplifier 3 of the Astra facility became operational in 1999 [1)], and has been in more or less continuous operation ever since. The development of Astra Gemini, with its requirement for better-quality input pulses and higher energy, was the driving force behind changes to Amp 3 made in 2006 [2)]. These changes included a two-level layout for beam expansion. Although this was undesirable for reasons of stability and accessibility, it was necessary because the large footprint of the Macholite pump laser severely limited space on the table. In the past year that laser has been replaced with four Quanta-Ray lasers which are positioned to one side of the amplifier table, releasing a large amount of space on the table itself. This change provided an opportunity to redesign the amplifier layout and return to a single level. Here we describe the changes made to the amplifier and its infrastructure and present results demonstrating its performance.

New pump lasers and cooling system

The Continuum "Macholite" laser was a customized two-beam Nd:YAG laser producing up to 2.5 Joules of second harmonic light per beam at 10 Hz. In recent years this laser had become increasingly unreliable, being responsible in its final year for nearly half of the lost time on Astra. The new Quanta-Ray lasers each produce a single beam of 1.4 Joules at 532 nm at 10 Hz (1.3 Joules when injection-seeded), so the total available pump energy is 5.2 Joules, slightly higher than before. Another Quanta-Ray laser has been used for many years in Astra to pump the second amplifier, and has proved the most reliable of all the commercial lasers used in the facility.

The cooling water for the Macholite was supplied by a complex system with three circuits, which was hard to access and also prone to faults. To cool the new lasers a completely new cooling system has been installed, with a new external chiller and properly-designed pipework that includes a filter, flow-meter and temperature gauge for each laser. The distribution pipework is mounted on an extension of the gantry that runs the length of the Astra laser area, as are the power sockets for the four lasers.

The lasers themselves stand on breadboards mounted on custom frameworks alongside the amplifier table. Each breadboard has two laser heads side by side, with their power supplies beneath them. The space between the frames is large enough for one power supply to be pulled out for maintenance when required, and the same space allows the laser operators access to the amplifier table for alignment.

Amplifier design changes

In redesigning the amplifier, we took the opportunity to change several of the less satisfactory aspects of the original design. The spatial filters between passes 1 & 2 and 3 & 4 were replaced with a better version based upon the successful design used in the Gemini amplifiers. In this the pinhole is mounted in a fixed position on a base plate that is clamped to the table, and a removable cover with a top viewing window is fitted over it. The beam tubes of the spatial filter have independent supports. The beam is aligned through the lenses and windows of the spatial filter and referenced to the kinematic crosswires at either end. The pinhole is then positioned so it is centred on the beam (at low power), and finally the cover is placed over the baseplate and the beam tubes joined to the sides. The same achromatic lenses were used as in the old amplifier; these are mounted on slides so the focusing can be adjusted once the spatial filter is under vacuum.

Another change from the previous layout was to allow more space around the TiS crystal holder. It was anticipated that at some stage a cryogenically-cooled crystal might be used in this amplifier, which would need more space, so the beam angles through the crystal were increased slightly, and the spatial filters are a few centimetres further from the crystal mount.

With the pump lasers mounted to one side of the amplifier table there is enough space available to position the entire amplifier so it lies on a single table, rather than straddling across two tables as in the previous design. This allowed the heights of all the components to be preset to the beam height of 110 mm, which ensures the beams are horizontal everywhere.

Pump beam distribution

As there are now four pump beams rather than two, the design of the pump beam expansion and distribution system had to be changed significantly from the previous arrangement. The beam expansion factor from 12 mm to 18 mm is the same as before, but space constraints meant that the focal lengths of the expander lenses had to be shorter, and it was no longer possible to use nitrogen-filled pipes to enclose the focal regions as there would always be breakdown at the foci. We decided to use vacuum pipes of large enough diameter that two beams could be expanded in each pipe side by side. Two of the beams have further to travel, so their expansion optics are of longer focal length. The optics of all four beams are designed to image-relay a plane near the output of the laser onto the crystal, to ensure the illumination of the pumped region is as uniform as possible.

In practice, the windows of these expander tubes caused significant problems. Despite the use of an oil-free pump in the vacuum system, the antireflection coatings on the insides of the windows gradually became contaminated, which led to the coating degrading and eventually being burned off the substrate. The resulting loss of energy compromised the performance of the amplifier until the window was rotated to a new position. At the time of writing, new window assemblies for uncoated Brewster-angle windows are being manufactured, and it is expected that these will resolve the problem.

As in Gemini, the pump beams are on a higher level than the seed beam, 150 mm rather than 110 mm, so pass through the crystal travelling slightly downwards. The transmitted beams are collected on four (plane) recycling mirrors, which retro-reflect them back to the crystal. There is a significant benefit to pump recycling, as the crystals used in this amplifier typically transmit about 7% of the pump light, which would otherwise be wasted. A similar scheme is used in the Gemini amplifiers.

Amplifier layout

The layout of the amplifier and new pump lasers is shown in Figure 1. All the design drawings were made using a 3-D CAD program to ensure none of the hardware components obstructed any of the beams. In laying out the components, a full-size printout of the base layout was fixed to the table, and cut-outs made for the mount bases and other items to allow accurate positioning. This procedure saved a great deal of time, as the design ensured there were no unresolved alignment issues. With the optics positioned according to the drawings, it was easy to align the beam through the amplifier, with only minimal changes to component positions. In the figure, the four pump beams are shown in red, yellow, green and blue, and the 800 nm seed beam in purple. To avoid cluttering the diagram, only representative components are labelled.

As before, the beam makes four passes through the TiS crystal, with a vacuum spatial filter between the first and second passes and another between the third and fourth. After the final pass it is expanded to 31 mm diameter, as required for propagation to Gemini. Energy controls in the form of a waveplate/polarizer combination and slide-in attenuator mirrors, plus a fast shutter, allow the users to set the shot energy and fire shots on demand, or to use the 10 Hz beam at low or medium energy.

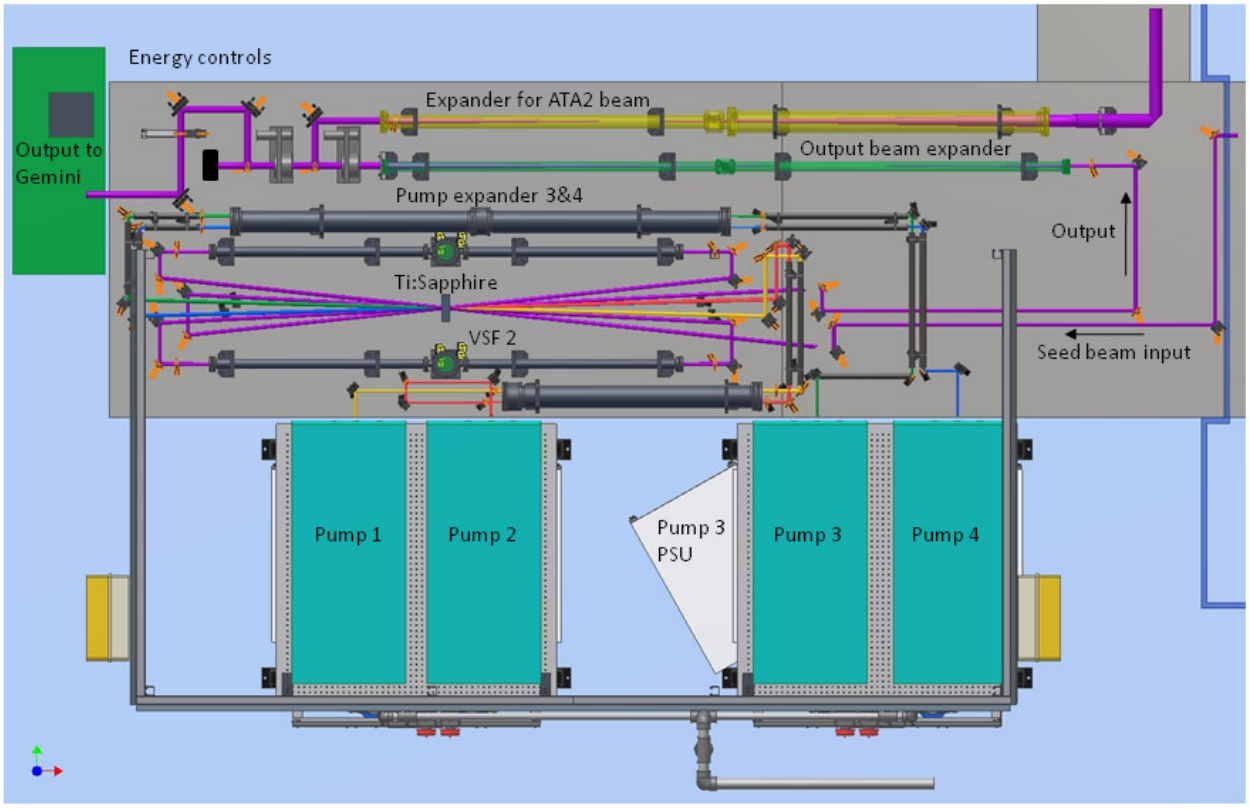

Figure 1. Schematic layout of new Astra Amplifier 3.

Triggering and timing

Each of the lasers requires a trigger to fire the lamps and another to fire the Q-switch. The requirement to adjust these independently and in groups led to a redesign of the scheme that was used for the Macholite. The new scheme uses three Stanford delay generators (DG535): one is the master delay box, and is triggered by a 10 Hz signal from the front end. Two of its outputs are used to trigger the other two boxes, which drive the four lamp triggers and the four Q-switches respectively, via their four main outputs. The Q-switch trigger channel is set up as the sum of two delays (B + constant); the B delay is zero for normal operation but is increased to 1 microsecond for alignment, so the crystal is thermally lensed but does not give any gain. Changing the trigger delays on the master box allows the timings of all the lasers to be adjusted together, and the separate delays on the lamp and Q-switch boxes allow the timings of each laser to be optimized individually.

Automatic alignment

The automatic alignment system used in the first two amplifiers has not yet been extended to Amplifier 3. However, the fast pointing control system [3)] has been reinstalled, as this improves the stability of the of the beam when it enters the Gemini laser area. It consists of a 2-inch mirror mount with three piezoelectric actuators (of which only two are used), and a far-field imaging system. The piezo-mounted mirror is the last optic before the final pass of the amplifier, and the far-field monitor receives the leakage beam transmitted through the next mirror in the chain, where a lens and a microscope objective focus the beam onto a fixed camera. There are no reflections between the piezo mirror and the camera, so the setup provides an absolute pointing reference. When active, the control software drives the piezo mirror to keep the far-field centred on the reference position, except when thermal changes force the piezo voltage out of range, at which point a manual correction of the mirror becomes necessary.

Environmental and beam enclosures

To protect the beams from air currents, some form of enclosure is essential. It is also necessary to protect the operators from the beams, especially the four pump beams which are a skin hazard as well as an eye hazard. The pump beams are enclosed in aluminium beam tubes as far as possible, as are the seed beam paths, but in the region around the crystal the overlap of paths makes this impossible. An environmental enclosure was designed, consisting of an extruded-aluminium framework with sliding and hinged Perspex panels, some with anodized aluminium skirts to block stray beams. The enclosure was installed only after the construction of the amplifier was

complete and the beams had all been aligned. A 50 mm wide gap was left along the top of the enclosure to allow cables and power leads to be fed through to equipment on the tables. Figure 2 shows part of the amplifier after the environmental screens had been installed: the four pump lasers are visible on the right, with the expander pipe for beams 1 & 2 and the smaller tube of the second VSF. The TiS crystal in its holder is visible on the left, along with two beam dumps on pneumatic slides which are used to dump the pump beams while the lasers are warming up.

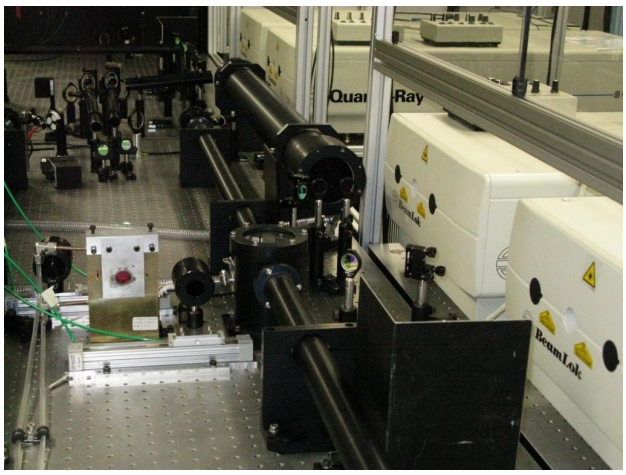

Figure 2. The new pump lasers and part of the completed amplifier.

Amplifier performance

The pump lasers were installed and commissioned in July 2009, and met their energy specification of 1.3 Joules per pulse at 532 nm. After a shakedown period, the alignment of the amplifier proved to be very stable from day to day, and the output energy was typically between 1.2 and 1.3 Joules with a reasonably uniform near-field profile (see Figure 3 below). The far-field shows a small amount of astigmatism; this is caused by the oblique passage of the beam through the thermally lensed crystal, and was also seen in the original design of the amplifier.

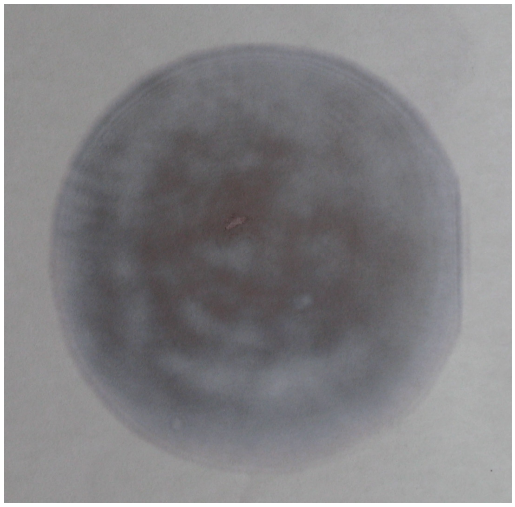

Figure 3. Burn pattern of 31 mm output beam.

New interlock system

While the upgrade of amplifier 3 and its infrastructure was in progress, the old PC-based interlock system was stripped out and replaced by a modern version using PLC technology. The old system was installed at the time the original Astra facility was set up, and some of the computers running the system software dated from around 1999 or 2000. Concerns about reliability and the lack of spares made a compelling case for replacing them with a modern interlock system similar to the ones developed for Gemini, Astra Artemis and other areas of the CLF. As with all the modern systems, the user interface is via Magelis touch screens rather than mechanical switches and buttons, but authorization keys are still required and are issued to operators so they can gain entry to the areas and switch on hazardous devices. For the laser area entry door there are two parallel keyswitches, one of which is operated by the laser operator's key, and the other by a separate key for the users to enter the area when switching Astra off after operating during the evening. This second key cannot be used to switch on any of the lasers in the area, which provides an additional level of security against unauthorized operation of Astra. Linked to the interlock system is the display program, which runs the hazard display screens mounted outside the doors and at easily-visible places inside the areas. This new system covers the two Astra laser areas and also Target Area 2. There is no link to the Gemini interlocks, nor is one needed, because the interface between LA2 and LA3 consists of a single shutter in LA2. This shutter and its associated virtual shutter are controlled by the Gemini interlock system.

Conclusions

We have successfully completed a significant upgrade to Astra, which has removed one of the least reliable lasers from the system, and improved the layout and ease of access to the third amplifier. We have also replaced the increasingly unreliable PC-based interlock system with an up-to-date modern system that is compatible with similar systems elsewhere in the CLF.

Acknowledgements

The authors wish to thank the mechanical and electrical engineers of the CLF involved in this upgrade, whose efforts were vital in completing the work on schedule.

References

1. CLF Annual Report 1999-2000, pp196-200
2. CLF Annual Report 2006-2007, pp165-167
3. CLF Annual Report 2008-2009, pp 211-212

Improved post-experiment data analysis at Astra Gemini

Contact *victoria.marshall@stfc.ac.uk*

Victoria Marshall and Dan Symes
Central Laser Facility, STFC, Rutherford Appleton Laboratory, HSIC, Didcot, Oxon, OX11 0QX

Background

For the last few years Astra Gemini laser diagnostic data have been captured, processed and stored in a sizeable database. The "raw" data is already made available to users via NeXus[1] files and the eCAT and penguin applications (described in earlier years of the CLF annual reports[2,3]), but with such a wealth of data available it is sometimes difficult to ascertain overall performance during the course of an experiment which can easily run to 1000 shots. We describe a recent addition to the penguin suite which aims to provide facility users (and laser operators) with a tailored digest of laser diagnostics to aid their own analysis.

Real-time data acquisition

The e-infrastructure set up for Astra Gemini ingests and stores a large amount of diagnostic data on a per-shot basis. The data currently comprises 500+ singular values (energies, pulse lengths, x- and y-positions, temperatures etc), 40+ images (compressed and uncompressed near- and far-field images, FROG images) and 200+ traces (spectrometer and scintillator traces), nearly 800 data streams in all. (There are also 20+ data streams of continuous data of vacuum pressures, crystal and ambient room temperatures, and pump energies.

Although specific requirements may vary for each experiment, there is usually a common subset of data channels of interest to the users. These can be chosen in consultation with the Principal Investigator and the data made available through the eCAT and/or penguin interfaces during experimental shots. Additionally the data, including singular values, trace images and camera images can be posted after every shot and made available as a web service. Figure 1 shows various laser parameters recorded for a series of shots in Comma-Separated Value (CSV) format. This CSV data can be downloaded and incorporated into analysis programs written for target area diagnostics. For example, a signal can be normalised to laser energy and plotted within seconds of the shot, enabling real-time assessment of data trends.

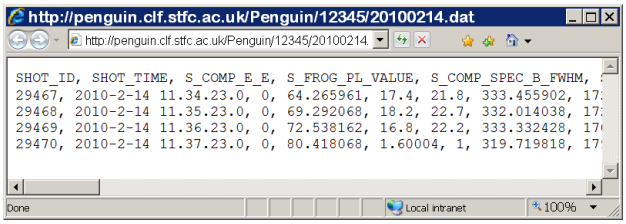

Figure 1: Extract from a CSV file.

Post-experiment analysis

The availability of laser performance data in a database allows CLF staff to carefully analyse the performance of the laser after an experimental campaign. This is crucial to pick up problems which may have been missed in day-to-day running. It also provides a valuable resource with which users can correlate experimental observations with deliberate or unintended changes in laser parameters. To this end, we are preparing reports in the penguin format which will be made available to the users soon after the end of the experiment. (These reports will not be posted to the public if there is any chance of a breach of confidentiality.)

Daily presentation of data

The data streams are presented as a shot-by-shot, day-by-day list of single values, traces and images. At the end of each day of experimental shots, singular value data streams are averaged and displayed following that day's shots. Traces are also averaged and displayed as a Scalable Vector Graphics[4] (SVG) thumbnail which can be clicked on to enlarge and view in greater detail. The raw data for the plot is also available.

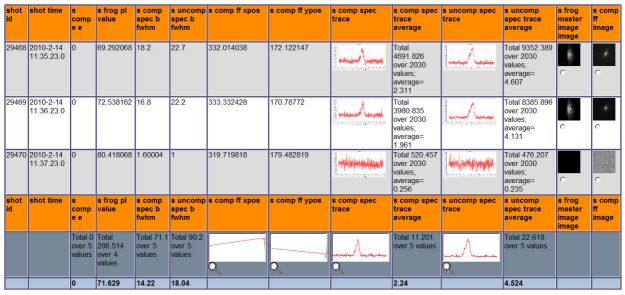

Figure 2: One day's shots extracted from the main display, showing raw and averaged data.

Summaries and representative data

The laser operator can subsequently view this data and, for image data streams such as far-field profiles and FROG traces, select the image which represents a typical image for that day. In this way we compile an overall summary table detailing, on a day-by-day basis, the average trace plots, the representative images and a scatter plot of X/Y position pairs. Following this is a table with the averaged singular data throughout the experiment and a list of all downloadable data (data, CSV and SVG files). The summary will be scrutinised by laser and target area operations managers, and any notable occurrences accompanied by a comment.

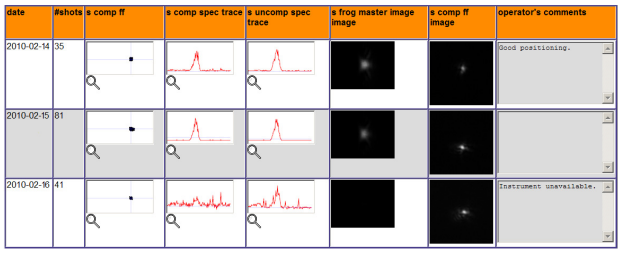

Figure 3: Three day's worth of representative images and plots.

References

1. http://www.nexusformat.org/Main_Page
2. **Laser performance data analysis tool**, EJ Divall, Central Laser Facility Annual Report 2007-2008, pp. 220-222
3. **eCLF project progress**, RJ Clarke, EJ Divall, R Pattathil, M Gleaves, L Lerusse, V Marshall, L Sastry, A Pakhira, Central Laser Facility Annual Report 2008-2009, pp. 209-210
4. http://en.wikipedia.org/wiki/Scalable_Vector_Graphics

A new phase (and amplitude) for Astra Gemini: Using a Spatial Light Modulator

Contact *chris.hooker@rl.ac.uk*

Chris Hooker and Victoria Marshall

STFC Rutherford Appleton Laboratory
Harwell Science & Innovation Campus
Chilton, Oxfordshire, OX11 0QX

Introduction

Maintaining uniform spectral phase is essential in chirped-pulse laser systems to ensure that the pulse can be recompressed correctly at the end of the laser chain. In a system with a grating compressor, second- and third-order phase errors can (in theory) be compensated by adjustment of the grating separation and the angle of incidence. Phase errors that remain require other means of compensation, typically by an acousto-optic modulator such as a Dazzler. Spectral phase errors in the Astra/Gemini laser chain are at present corrected by means of a Dazzler positioned in the kHz preamplifier (Compact Pro). This device has several troublesome characteristics that reduce its effectiveness; in particular there appears to be a linkage between phase modulation and spectral modulation. If the amplitude of the phase correction exceeds a relatively small amount at any wavelength, or if the variation in applied phase correction with wavelength is too rapid, the result is a modulation of the spectral amplitude over the entire bandwidth. Many ultrashort-pulse laser systems use spatial light modulators (SLMs) to control spectral phase and amplitude independently. The advantage of such devices is that the light is dispersed at the point where the modulation is applied, which minimises the chance of a correction at one wavelength influencing what happens elsewhere in the spectrum. We report on the design and construction of an SLM-based phase correction arrangement for Astra Gemini.

Spatial light modulators

Spatial light modulators use arrays of liquid-crystal elements mounted between transparent electrodes. When a voltage is applied between the electrodes, the refractive index of the liquid crystal is altered, changing the optical path through that part of the modulator and thereby altering the relative phase of the light passing through it. If a broadband laser pulse is dispersed so that each element of the SLM array passes a small region of the spectrum, the relative phase of each part of the spectrum can be adjusted freely by applying different voltages to each element.

For our application we selected an SLM array made by Cambridge Research and Instrumentation, Inc (CRI), which has two liquid crystal cells mounted together between parallel polarizers. Each cell has 128 pixels of 100 microns width; the active part of the array is thus 12.8 mm across. The two cells are registered within 1 micron, so each pixel of the SLM array consists of two cells in series. The idea behind this is that it allows independent phase and amplitude control. The phase correction is determined by the average (or the sum) of the voltage values applied to the two cells of a particular pixel. If there is a difference between the voltages, this results in a rotation of the polarization and hence reduced transmission through the exit polarizer, thus modulating the spectral amplitude. The maximum phase difference that can be applied with this array is 3 radians, an amount that causes severe spectral modulation if applied with the Dazzler.

SLM optical configuration

For the SLM to work correctly, the light must be dispersed at the plane of the modulator, so corrections can be applied to narrow wavelength regions. The dispersion must then be reversed to restore a collimated beam. The standard technique for doing this is a so-called '4F' system, in which the input beam, which is collimated, is dispersed by the first grating into a spread of directions. This fan of light is collected by an achromatic lens positioned one focal length F from the grating, so that the ray bundles of each wavelength are made parallel. Each bundle, however, is focused by the lens so that a well-resolved spectrum is formed at a distance F beyond it. This is the plane where the SLM is located, 2F from the first grating. Beyond the SLM, a mirror-image setup with another achromat and grating reverses the spatial chirp to restore an undispersed beam.

Our SLM has a width of 12.8 mm and a period of 100 microns; there are thus 128 active elements. Calculations based on a bandwidth of 100 nm full-width showed that a grating with 600 grooves per mm, combined with lenses of 200 mm focal length, would produce a spectrum that fitted comfortably within the SLM and used most of the pixels. Gratings of that groove density are readily available as replicas of ruled, blazed, gratings, with first-order efficiencies up to 90%, an important consideration to avoid loss of energy. Suitable achromats corrected for the near-infrared are available off-the-shelf from various suppliers, e.g. Thorlabs.

The SLM array is mounted in a large housing at a height incompatible with the 110 mm beam height of Astra. However, the modulator requires the beam to be horizontally polarized, and the gratings are also most efficient in the same polarization. Accordingly, the beam from the Astra pulse stretcher was raised to a height of 180 mm and turned through 90 degrees with a 2-mirror periscope, thereby changing the polarization and reaching a suitable height for the SLM. A second periscope after the 4F optics returns the beam to its original height and polarization and directs it into the original beam path. The setup was designed so that the SLM could be bypassed simply by moving the two lower periscope mirrors out of the path.

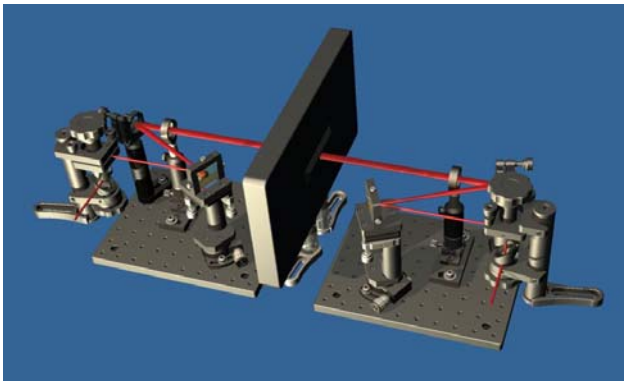

Figure 1. Design drawing of the 4F SLM optical setup

A schematic of the design is shown in Figure 1. The final setup is slightly different, in that the periscope optics are also mounted on the breadboards. The device is now bypassed by simply sliding the two breadboards towards one another by 20 mm: this allowed the 4F optics to be set up during the warm-up period of the laser each morning when the beam was not required, without disturbing the alignment of the laser in any

way. The cameras of the autoalignment system proved invaluable in ensuring that the 4F setup was adjusted correctly, because the image sizes and positions are very sensitive to errors in beam collimation and pointing. One issue that was noted is that the 4F optics invert the beam: this has the effect that the autoalignment system becomes unstable, as a correction applied before the 4F setup causes the spot to move away from the reference position on any camera downstream of the SLM. When the SLM is finally made a permanent part of the system, the auto-alignment software will have to be 're-trained'.

Control program and user interface

The SLM is controlled via ASCII commands using a high-speed USB interface. Two 128-pixel masks are available, which can be controlled independently to effect phase and/or intensity modulation. Figure 2 below shows the screen of the user interface.

Firstly, the operator needs to define the masks.

Polynomial phase settings: Four polynomial phase settings are available: K_1x, K_2x^2, K_3x^3 and K_4x^4. These can be controlled independently using sliders and are plotted separately in the top graph. Their combined values are shown in the combined phase pattern plot below it. All values are taken modulo 2048; *i.e.* they are wrapped if their values go outside the range ± 2048.

Local phase settings: These are defined by small groups of pixels (usually in groups of three) and defined using the two bitwise sliders. To create a phase hole, the operator chooses the position with the horizontal slider and the amplitude with the vertical one. A Gaussian function is used to smooth the curve. These local corrections are summed, then plotted both separately and combined with the polynomial values. For pure phase corrections the same voltage is applied to each mask.

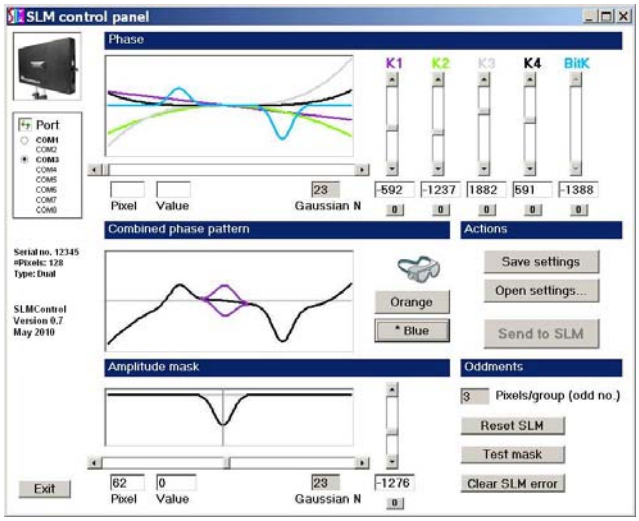

Figure 2. Screen image of the SLM user control interface

Amplitude settings: These are defined at the bitwise-level using the lowest plot and two sliders, and by applying a Gaussian function. The voltages applied to each mask are adjusted to the required difference, so that their combined value (which controls the phase correction) is unchanged. The effect is shown on the combined plot. In this way a spectral hole of any desired width and depth can be created.

Once the operator has defined the masks to be used, they can be downloaded to the SLM itself using the "Send to SLM" button. Settings can also be saved to and restored from XML files.

One complication was the requirement to be able to use the SLM interface while using safety goggles which restrict visibility as well as colour range. There are two types of goggles in common use, one transmitting in the orange part of the spectrum and one in the green-blue. This was solved using two sets of colour tables and a button to swap between them. Both versions appear slightly unusual to the naked eye, but more importantly they are usable wearing goggles in a laser laboratory with high-power laser hazards present.

Results and further work

Only brief preliminary tests have been carried out so far. However, the device was shown to be capable of modifying the spectrum from Astra with a resolution significantly better than the Dazzler. The depth of modulation was essentially 100%, i.e. a chosen part of the spectrum could be completely blocked. We have not yet had an opportunity to try controlling the phase at the output of Gemini using the device. The intention is to retain the Dazzler, primarily as a means of controlling the spectral bandwidth from the front end. Assuming the SLM works as expected, it will become the primary means of phase control, and a secondary means for adjusting the shape of the spectrum that enters the Astra amplifier chain. There is also an option in the SLM to store more than one set of masks, and to switch between them if the laser is running in alternating single- and double-stretch mode.

Ultrafast gated imaging of laser produced plasmas using the optical Kerr effect

Contact *dan.symes@stfc.ac.uk*

D. R. Symes, U. Wegner, H-C. Ahlswede, M. J. V. Streeter, P. L. Gallegos, E. J. Divall, P. P. Rajeev, D. Neely
Central Laser Facility, STFC, Rutherford Appleton Laboratory HSIC, Didcot, Oxon OX11 0QX, UK

R. A. Smith
Laser Consortium, The Blackett Laboratory, Imperial College London, Prince Consort Road SW7 2BZ, UK

Introduction

Optical probing is a powerful diagnostic tool which is frequently used for high energy density plasma experiments with high power lasers. It enables the measurement of plasma electron density[1] and visualization of energy transport and shock propagation [e.g. Ref. 2]. Short (<1ps) laser pulses can be employed as a backlighter for transverse imaging of the interaction with a temporal resolution limited by the transit time of the pulse through the plasma. The emission of light created by the laser-matter interaction can also be imaged: both the nanosecond timescale radiation from the directly heated plasma and also short bursts of harmonic or transition radiation emitted as relativistic electrons leave the target[3]. The resolution for these measurements is determined by the exposure time of the camera, which can be electronically gated to be on the timescale of ~100 picoseconds. The gate can be timed to eliminate the majority of the self-emission from the plasma which causes a problematic background in high intensity experiments. The detector response can be made faster by driving the gate optically rather than electronically by incorporating into the imaging system an optical Kerr gate (OKG). This is composed of two crossed polarizers around a non-linear medium[4] which is opened by passing an intense laser pulse through the gating medium to introduce a polarization rotation to the probe pulse allowing it to reach the detector. The OKG is used extensively for spectroscopic applications[5-8] and is a standard technique within the LSF. It has also been employed for ballistic-photon imaging[9-11], laser contrast improvement[12] and is the basis for polarization gated frequency-resolved optical gating used to diagnose laser pulses[13]. Carbon disulfide is commonly used for the gating medium because of its strong non-linear response but it has a slow relaxation time ~1ps. For ultrafast applications, glass or crystals must be used because of their much faster response[6,7] but these usually need higher laser intensities to induce the necessary birefringence.

Design of the Kerr gated imaging system

We report on the application of Kerr gating to the imaging of laser-produced plasmas on Astra[14,15]. We present shadowgraphic images of the laser interaction with a solid target to demonstrate the suppression of background light from plasma self-emission, which otherwise dominates the image. We also discuss the exceptional performance that should be achievable with further optimization of the imaging system. The gated imaging scheme comprised a four lens system which image relayed the plasma interaction to the position of the OKG and then re-imaged with magnification to the charge-coupled device (CCD) camera. A linearly polarized probe beam was used as a backlighter, which was split before the CCD and focused onto a photodiode to monitor gating performance. Short pass filters were used to block light at the fundamental 800nm wavelength. The OKG was formed by aligning a collinear gating beam with its polarization oriented at 45° to the probe through a non-linear medium and placing a polarizer in front of the detectors. The experiment was performed in Astra Target Area 2 using the output from the hollow fiber pulse compressor (HFPC)[16,17] to provide a good spatial profile. The fiber was operated without a gas fill, preventing spectral broadening and so the pulse duration remained at ~60fs. A second harmonic (400nm) probe pulse was generated in a thin β-Barium-Borate crystal and the remaining 800nm light was used as the gating beam. This was focused to 1mm diameter at the OKG, generating sufficient intensity to drive the gate while remaining large enough to provide an adequate field of view for plasma imaging.

Characterisation of the Kerr gate

We investigated the properties of the gated imaging system by measuring the transmitted 400nm signal. To ensure the entire probe beam experienced polarization rotation, its size at the OKG was made smaller than that of the gating beam. We tested two glasses as gating materials: fused silica (FS) and Schott NSF-66. These samples were 1mm thick, 1 inch diameter windows and the FS had a broadband antireflection coating. Both glasses are inexpensive and FS is well known to have an instantaneous (~1fs) response[13]. The high-index NSF-66 (1.914 at 632.8nm) was chosen because the effect is expected to be stronger with increasing linear refractive index[6].

The signal as a function of the gating beam intensity is shown in the inset to Fig. 1 for FS. The Kerr effect becomes significant once the intensity exceeds 8×10^{10} Wcm^{-2} (150μJ) and follows a quadratic dependence with increasing energy (as seen in Ref. 4) until ~2.5×10^{11} Wcm^{-2} (500μJ). The transmission is ~20%, which seems reasonable since the intensity required to drive a half-wave polarization rotation of the probe is ~ 7.5×10^{11} Wcm^{-2}. In NSF-66, the maximum intensity was limited by the onset of white light generation by the gate pulse causing saturation of the CCD camera. At this intensity, the efficiency of NSF-66 was only slightly higher (~23%) than the FS.

The transmission for both materials is plotted against the gating beam delay in Fig. 1. In NSF-66 the birefringence endures for ~1.5ps precluding ultrafast gating. In contrast the FS gate

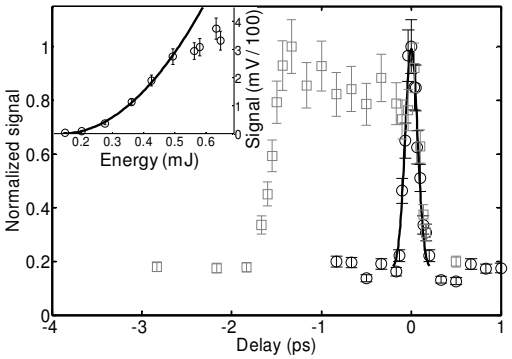

Figure 1. Probe signal as a function of gating beam delay using as the Kerr medium fused silica (black) and NSF-66 (gray). The inset shows probe signal versus gating beam energy for the fused silica gate.

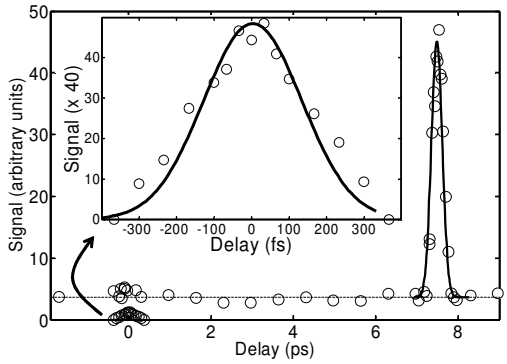

Figure 2. Gated measurement of a strong (7.5ps) and a weak (0ps) probe pulse. The dashed line indicates the background level caused by the strong pulse. The inset shows the weaker pulse measured with no strong pulse present (signal x 40).

transmission is fitted with a full width half maximum of 180 fs. Given that FS is known to have ~fs response time the duration of the gate should be limited only by the gate duration of ~60fs. However, since the gate is short, the signal width that we measure is determined by the duration of the probe pulse which is lengthened because of transit through ~8mm of glass. In future work we intend to conduct a more sophisticated measurement of the gate duration.

We measured the dynamic range of the system by splitting the probe and attenuating one pulse by a factor of 50. Figure 2 shows a scan of the gating beam delay with the zero position defined as the peak of the weaker pulse. The attenuated pulse could be resolved in the absence of the stronger pulse (at 7.5ps), when the background level was negligible. With the stronger pulse present the background level increased to ~40mV (dashed line), almost obscuring the weak pulse. This ~7% background is caused by leakage of the strong pulse through the crossed polarizers which, in this arrangement, had an extinction ratio of 100.

Application of Kerr gating to plasma imaging

Adding the OKG to the imaging system suppresses the level of plasma emission since this occurs on a nanosecond timescale compared to the ~100fs timescale of both the gate and the probe beams. In high intensity interaction experiments this background is problematic because it necessitates a correspondingly bright probe beam. The use of gated imaging relieves this requirement. We demonstrated background reduction by recording shadowgraphic images of plasma formation in a 100 µm thick glass target irradiated at ~2.5 x 10^{14} Wcm^{-2} by 2mJ, 60fs laser pulses focused to a 70 µm spot. At this intensity the single-shot emission was not bright compared to the probe beam so we used multiple laser shots to create damage craters with complicated structure which lead to greater laser absorption[18]. A series of 100 laser shots was incident onto a thin glass target (a movie of this is available on request). Without gating after about 20 shots the self-emission became much brighter and saturated the camera, obscuring the interaction region. In contrast, the use of the OKG enabled clear imaging of the structure of the glass and diagnosis of the emergence and propagation of cracks. Recording a sequence of 250 shots allowed us to observe the laser drilling completely through the target (movie available). The results are shown in Fig. 3 which shows irradiation of the crater after 25 shots (a) without and (b) with optical gating, with a probe delay of 2.5ns. In (a) the interaction region is obscured by self-emission whereas this background is not seen on the gated detector in (b).

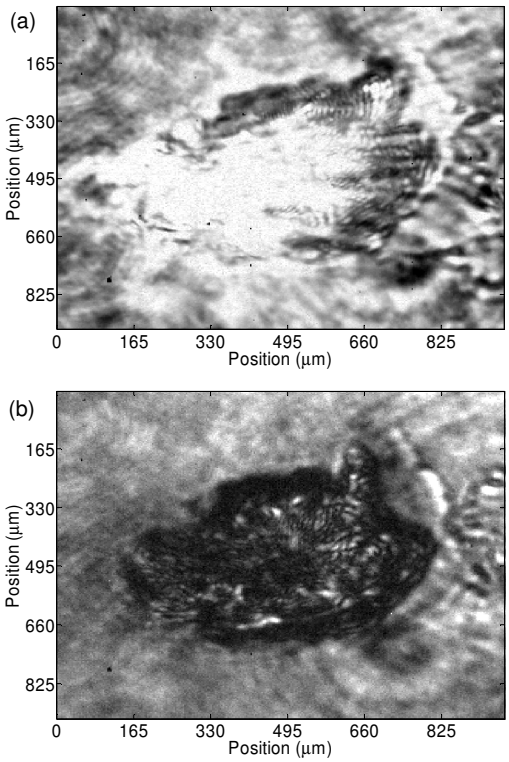

Figure 3. Shadowgraphic images of a glass target irradiated at laser intensity 2.5 x 10^{14} Wcm^{-2} at a probe delay of 2.5ns (a) without and (b) with optical gating. The target has previously been subjected to 25 laser shots to enhance plasma self-emission.

Alternative gating materials

As well as the two glasses we tested two alternative gating materials which have previously been used in fast-response OKG systems: zinc oxide[19] and lead-bismuth-glass (LBG)[12,20]. When we used ZnO we found that rather than inducing the polarization rotation necessary for gating, the intense gating pulse induced a strong absorption of the 400nm probe pulse as shown in Fig. 4. This makes it inappropriate for Ti:sapphire second harmonic probing but it should be usable for other probe wavelengths. Importantly, the use of this ZnO wafer had no detrimental effects on the image quality, Fig. 5(a), so we can employ different crystalline materials[7] for 400nm

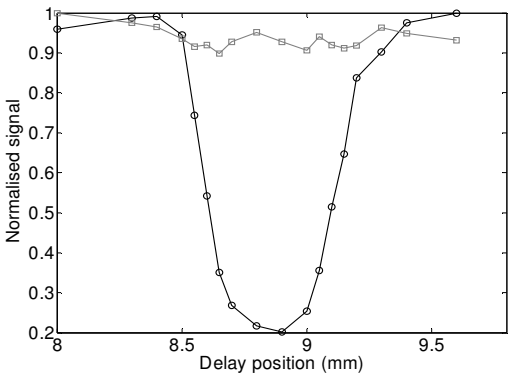

Figure 4. Probe signal (black) as a function of gating beam delay using ZnO as the Kerr medium with fluctuations in the infrared pulse energy shown (gray).

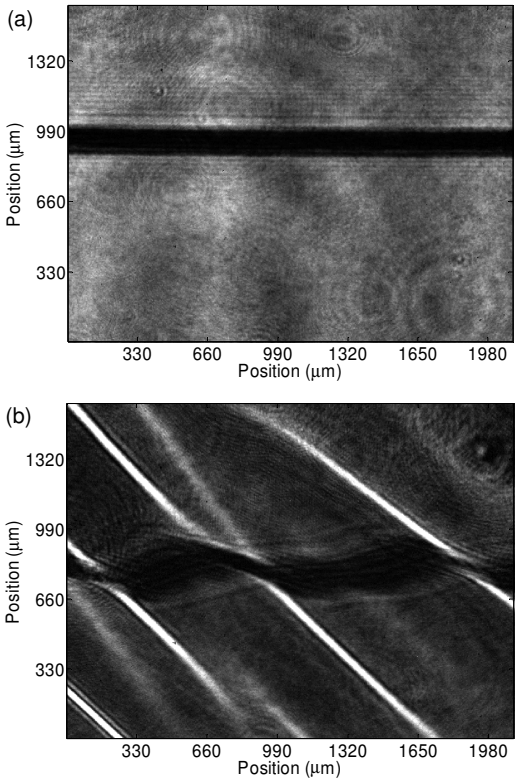

Figure 5. Imaging of a wire through (a) zinc oxide wafer and (b) lead-bismuth-gallium glass. Structure in the glass prevents the use of this sample for an imaging application.

probing. This should be compared to the image in Fig. 5(b) obtained using the available sample of LBG, which introduced striations to the image highlighting the need for good quality glasses for these imaging applications.

Conclusions

We have demonstrated that high speed optical Kerr gating can be incorporated into the imaging systems commonly used for diagnosing high energy density plasmas created using intense laser pulses. We have presented images which show the effective elimination of plasma self-emission from the camera. This is of great benefit for experiments using ultra-intense laser systems in which this background constitutes a common problem. These images also highlight the potential of the optical gating technique for investigations of material properties, such as in situ laser optic damage testing[21]. The gating beam can be tilted with respect to the probe[13,22,23] to convert the device to an ultrafast all-optical streak camera. These instruments will thus constitute low-cost plasma diagnostics with substantially higher dynamic range and superior temporal resolution than current generation electro-optic devices.

In principle, the gated system should be capable of an instrument response on a sub-10fs timescale and optimizing the performance remains a challenge requiring further research. It should be noted that even without an ultrafast response, optical gating on the picosecond timescale, using conventional gating materials (CS_2) and low intensities (5 GW cm^{-2}) can be used for background suppression in high intensity experiments. We aim to introduce optically gated imaging as a standard diagnostic for high power laser experiments within the CLF.

Acknowledgements

We acknowledge useful discussions with P. Matousek, J. Collier, I. Tracey, K. Ronayne and U. Teubner. We thank the Astra laser operators and target fabrication team. Sections of this report and figures 1 – 3 & 5 were adapted with permission from Ref. 14, ©2010, American Institute of Physics doi:10.1063/1.3279139.

References

1. I. H. Hutchinson, *Principles of Plasma Diagnostics* (Cambridge University Press, Cambridge, 1987).
2. B. A. Remington, R. P. Drake, and D. D. Ryutov, *Rev. Mod. Phys.* **78**, 755 (2006).
3. J. J. Santos, F. Amiranoff, S. D. Baton *et al*., *Phys. Rev. Lett.* **89**, 025001 (2002).
4. P. P. Ho and R. R. Alfano, *Phys. Rev.* A **20**, 2170 (1979)
5. P. Matousek, M. Towrie, A. Stanley, and A. W. Parker, *Appl. Spectrosc*. **53**, 1485 (1999).
6. S. Kinoshita, H. Ozawa, Y. Kanematsu, *et al*., *Rev. Sci. Instrum.* **71**, 3317 (2000).
7. R. Nakamura and Y. Kanematsu, *Rev. Sci. Instrum*. **75**, 636 (2004)
8. B. Schmidt, S. Laimgruber, W. Zinth, and P. Gilch, *Appl. Phys.* B **76**, 809 (2003).
9. R. R. Alfano, X. Lian, L. Wang, and P. P. Ho, *Science* **264**, 1913 (1994).
10. C. Dunsby and P. M. W. French, *J. Phys. D: Appl. Phys*. **36**, R207 (2003).
11. J. B. Schmidt, Z. D. Schaefer, T. R. Meyer, et al., *Appl. Optics* **48**, B137 (2009).
12. J. Collier, E. Divall, and I. Ross CLF report 2003/2004 p. 194; E. J. Divall, J. L. Collier, and I. N. Ross CLF report 2004/2005 p. 222.
13. D. J. Kane and R. Trebino, *Opt. Lett.* **18**, 823 (1993).
14. D. R. Symes, U. Wegner, H. –C. Ahlswede, *et al*., *Appl. Phys. Lett*. **96**, 011109 (2010).
15. L. Savage, *Photonics Spectra*, March 2010.
16. J. S. Robinson, C. A. Haworth, H. Teng, *et al.*, *Appl. Phys*. B **85**, 525 (2006).
17. D. R. Symes, E. J. Divall, P. S. Foster, *et al*., CLF report 2007/2008 p. 246; D. R. Symes, E. J. Divall, and U. Wegner CLF report 2008/2009 p. 228.
18. R. V. Volkov, D. M. Golishnikov, V. M. Gordienko, *et al*., *JETP Lett*. **72**, 401 (2000).
19. V. V. Yakovlev, *Spectroscopy*, **22**, 34 (2007).
20. B. L. Yu, A. B. Bykov, T. Qiu, *et al*., *Opt. Commun*. **215**, 407 (2003).
21. G. M. Guss, I. L. Bass, R. P. Hackel, *et al*., *Appl. Optics* **47**, 4569 (2008).
22. J. Shan, A. S. Weling, E. Knoesel, *et al*., *Opt. Lett.* **25**, 426 (2000).
23. Y. Kawada, T. Yasuda, H. Takahashi, and S. Aoshima, *Opt. Lett.* **33**, 180 (2008).